APPLICATION OF A TUNABLE ELECTROMAGNETIC DAMPER IN SUPPRESSION OF STRUCTURAL VIBRATION

Kefu Liu, Jie Liu and Liang Liao
Department of Mechanical Engineering, Lakehead University
Thunder Bay, Ontario Canada P7B 5E1
Contact: kliu@lakeheadu.ca

Received October 2004, Accepted February 2006
No. 04-CSME-49, E.I.C. Accession 2839

Abstract

An electromagnetic damper is developed to construct a tunable damped dynamic vibration absorber. The developed vibration absorber can suppress vibration of a structure subjected to a harmonic force with variable frequency. The damping of the vibration absorber can be adjusted on-line to cope with variation in the exciting frequency. The electromagnetic damper is composed of an electromagnet and a copper plate attached to the absorber mass. The relationship between the damping ratio and the damper current is discussed analytically. An experiment is conducted to determine the damping coefficients. A clamped-clamped beam is used as a primary system. The damper is connected between the absorber mass and the ground. This setup is referred to as skyhook dynamic vibration absorber in this study. The performance of a skyhook dynamic vibration absorber is compared with that of a groundhook dynamic vibration absorber where a damper is connected between the primary mass and the absorber mass. Two algorithms are proposed to tune the damper on-line. The first algorithm is FFT-based while the second one is rms-based. The control algorithms are tested against three frequency varying scenarios: multi-step change, linear change, and single-step change plus impact disturbance. Merits of each of the control algorithms are demonstrated.

APPLICATION D'UN RÉGULATEUR ÉLECTROMAGNÉTIQUE ACCORDABLE DANS LA SUPPRESSION DE VIBRATIONS STRUCTURALES

Résumé

Un régulateur électromagnétique est créé pour construire un amortisseur de vibrations dynamique accordable amorti. L'amortisseur de vibrations créé peut supprimer la vibration d'une structure soumise à une force de vibrations à fréquence variable. L'amortissement de l'amortisseur de vibrations peut être ajusté en ligne pour composer avec la variation de la fréquence excitante. Le régulateur électromagnétique est constitué d'un électroaimant et d'une plaque de cuivre attachés à la masse de l'amortisseur. Le lien entre le ratio d'amortissement et courant du régulateur fait l'objet d'une analyse. Une expérience est réalisée pour déterminer les coefficients d'amortissement. Une poutre encastrée aux deux extrémités est utilisée comme système primaire. Le régulateur est connecté entre la masse de l'amortisseur et le sol. Cette installation porte le nom d'amortisseur de vibrations dynamique à chariot aérien dans la présente étude. Le rendement de cet appareil est comparé avec celui d'un autre amortisseur de vibrations dynamique à chariot au sol dont le régulateur est connecté entre la masse primaire et la masse de l'amortisseur. Deux algorithmes sont proposés pour accorder le régulateur en ligne. Le premier est basé sur une TFR et le deuxième, sur une valeur quadratique. Les algorithmes de contrôle sont testés en fonction de trois scénarios de fréquence variée : changement à plusieurs étapes, changement linéaire et changement unique plus perturbation d'impact. L'article présente également les mérites de chacun des algorithmes de contrôle.

1. INTRODUCTION

A dynamic vibration absorber (DVA) or tuned mass damper (TMD) is a passive device used to suppress vibration of a machine or structure excited by a harmonic force. The machine of interest is considered to be a primary system and the DVA is considered to be a secondary system. In theory [1], when the absorber natural frequency is equal to the exciting frequency, vibration of the primary system is completely eliminated. However, if the exciting frequency varies, vibration of the entire system may increase significantly. One of the solutions to variation in the exciting frequency is to make an absorber parameter tunable on-line. Tunable DVAs belong to semi-active or adaptive-passive vibration control devices. As reactive forces are used to suppress vibration, semi-active control devices consume less power than active control devices. Because of adaptability, the performance of tunable DVAs will not degrade due to a varying environment. Moreover, they can behave as passive devices in the event of loss of power; thus are reliable.

A typical DVA consists of a mass and a spring. A common choice for a variable element is the absorber stiffness [2-5]. When a DVA works at its design frequency, damping is considered to have an adverse effect on its performance. With the presence of damping, complete elimination of vibration at the design frequency cannot be achieved. Several methods have been proposed in order to actively remove damping effect such as the delayed resonator [6] and the piezoelectric actuators [7]. On the other hand, damper is deliberately introduced to obtain a damped DVA. A damped DVA will ensure an acceptable level of vibration at resonance whereas its performance at the design frequency is compromised. Therefore, ideally damping should be variable. In the case of conventional hydraulic fluid dampers [8, 9], a controllable orifice was used to alter the resistance to flow. The study reported in [10] used a variable friction damper to dissipate vibration energy and the damper's frictional interface can be adjusted by allowing slippage in controlled amount. In [11], a feasibility study was conducted on the use of the temperature dependent behavior of viscoelastic materials to achieve adaptable suppression band. Recently controllable-fluid dampers have been receiving great attention. Controllable fluids can reversibly change from a free-flowing, linear viscous fluid to a semi-solid with controllable yield strength in milliseconds when exposed to an electric (for electrorheological fluids) or magnetic (for magnetorheological fluids) field [12-14].

Compared with other types of damping, magnetic damping has several advantages: good linearity of damping characteristics, no mechanical contact, independence of temperature, cleanness, and usability in space, etc. In [15] a magnetic damper made of permanent magnets was used to control vibration of piping systems. In [16], a remotely tunable TMD with a magnetic damper was used to suppress vibration of large solar arrays. The tunable element is the absorber spring consisting of accordion flexures. The magnetic damper is made of a pair of permanent magnets whose gap can be adjusted manually. The study reported in [17] focused on effective restoring forces of the electromagnetic damping. In the study reported in [3], a magnetic damper was used to control vibration of higher modes of the beam. In [18], the methods of producing magnetic damping are classified as "motional emf (electromotive force)" and "transformer emf". Motional emf devices are based on the generation of emf due to a moving conductor within a stationary magnetic field. Transformer emf devices are based on the generation of emf in a stationary circuit, due to a time-varying magnetic field linking the circuit. The study in [18] concluded that in almost all realistic situations, the motional emf designs have a greater damping efficiency than the transformer emf designs. Electromagnetic dampers based on the phenomenon of eddy current belong to the motional emf designs. In [5] an electromagnetic motional emf damper was developed to construct a tunable dynamic vibration absorber. Part of the study was reported in [19]. This paper reports two further results: analytical comparison of two different damped DVAs and experimental comparison of two different on-line tuning algorithms.

The paper is organized as follows. In Section 2, the developed damper and experimental set-up are introduced. In Section 3, a comparison of two different damped DVAs is given. In Section 4, two

control algorithms are presented and their performances are experimentally evaluated. In Section 5, the conclusions of the study are drawn.

2. ELECTROMAGNETIC DAMPER AND EXPERIMENTAL SYSTEM

Figure 1 shows a schematic of the experimental setup. A middle-carbon steel toroid is used as the core of the electromagnet (6). The cross section of the toroid is 23.5 mm (width) × 11 mm (height) and an opening of 3.5 mm is cut through the toroid to form the C-shaped core. Gauge 18 wire is used to wind a coil of about 1800 turns around the core. The resistance of the coil is 3.25 ohm. Placed between the two poles of the electromagnet is a copper plate (5) with a dimension of 40 mm (width) × 40 mm (height) × 1.5 mm (thickness). The copper plate is attached to a mass (4) which is held at the end of a cantilever beam (3). The cantilever beam is clamped on atop of a stand (2) which is mounted in the middle of a clamped-clamped beam (1). The clamped-clamped beam is made of aluminum (6601-T6) and has a dimension of 50.8 mm (width) × 1057 mm (length) × 5.08 mm (thickness). The electromagnet is held by a clamp (7) that is fastened to the ground. Another electromagnet (9) is used as a shaker. The force generated by the electromagnet interacts with a small permanent magnet (not shown) glued on the bottom of the beam such that a non-contact exciting force is generated. The shaker is driven by a power amplifier (B&K 2706). A current control circuitry for the electromagnetic damper was built in house. A PC computer is used to control the system. The Data Acquisition (DAQ) board is DS1102 from dSPACE. ControlDesk (dSpace) is used to interface between Simulink (Mathworks) and DS1102. Vibration of the clamped-clamped beam is measured by an accelerometer (B&K 4393V) (8). A charge amplifier (B&K Nexus2692) is used to condition the accelerometer signal. This signal is used for on-line control.

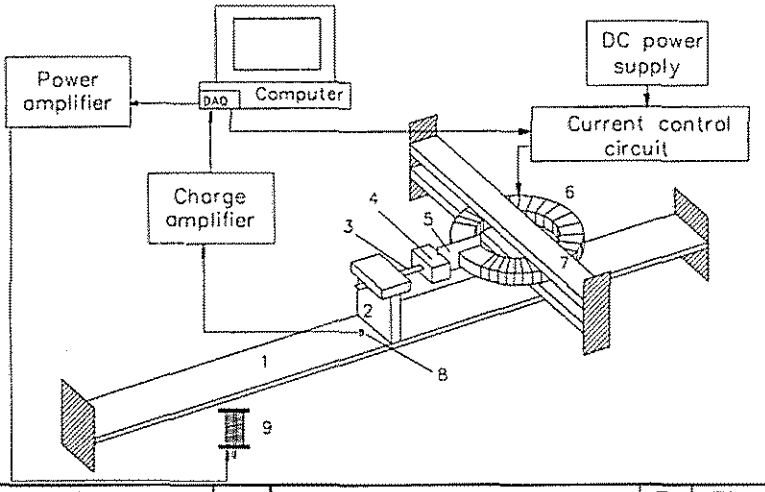

1	Clamped-clamped beam	4	Absorber mass	7	Clamp
2	Absorber stand	5	Copper plate	8	Accelerometer
3	Absorber beam	6	Electromagnet	9	Shaker

Figure 1. Experimental system.

The developed electromagnetic damper is based on the phenomenon of eddy current. To understand the damping mechanism, the motional emf principle is introduced briefly below. Figure 2(a) shows that a limited portion, Section O, of a plate or conductor made of a non-magnetic conductive material such as copper or aluminum is in a stationary magnetic field perpendicular to the plate. When the plate is moving downward shown in Fig. 2(b), an emf is induced in it. Sections M and N are not in the

field, thus provide conducting paths for charges displaced along O. The result is a circulation of eddy-like currents in the plate somewhat as sketched in Fig. 2(b). The currents within the field experience a magnetic force that opposes the motion of the plate. As the returning currents lie outside the field, they do not experience such forces. Therefore the interaction between the eddy currents and the magnetic field causes a retarding force on the plate.

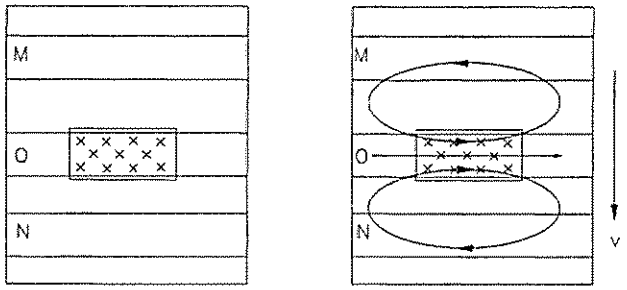

Figure 2. Eddy currents. (a) a stationary conductor in a magnetic field; (b) a moving conductor in a magnetic field.

Neglecting the inductance of the conductor, the damping coefficient c of a motional emf device is given as [15-18]

$$c = B^2 V/\rho \tag{1}$$

where B is the magnetic flux density, V is the volume of the conductor, ρ is the resistivity of the conductor. Neglecting flux fringing and leakage effects and the reluctance of the core, the flux density in the air gap of the electromagnet can be approximated by [20]

$$B = \frac{\mu_0 NI}{h} \tag{2}$$

where μ_0 is the permeability of the air, N denotes the number of turns in the coil, I represents the current through the coil, h is the air gap between the poles. It can be seen that the damping coefficient is related to the current by

$$c = \frac{V\mu_0^2 N^2}{\rho h^2} I^2. \tag{3}$$

Equation (3) is based on an ideal case. To understand the behavior of the developed electromagnetic damper, an experiment was conducted. The system was set up such that the mass was $m = 0.15$ kg and the natural frequency of the system was $f_n = 15.03$ Hz. With the coil current set to a constant value, an impact was applied to the absorber mass and the response was measured by an accelerometer placed on the absorber mass. For each given current, five tests were conducted. Using the measured acceleration signal, the damping ratio ζ was estimated by a curve-fitting method. The average of five estimated damping ratios was used. Figure 3 shows the relationship between the damping ratio and the damper current. In the figure, circles represent the damping ratios when the current was stepping up

from 0 A to 2.8 A in a step of 0.1 A while crosses represent the damping ratios when the current was stepping down from 2.8 A to 0 A in a step of 0.1 A. A fourth-order polynomial was used to curve-fit the data. It is noted that the quadratic relation between the damping coefficient and the current exists only for the small current magnitude. When the current magnitude increases, the varying trend is flattened out. This is mainly caused by the magnetic saturation in the ferromagnetic core. When the magnetic saturation occurs, the flux density B is no longer proportional to the current I, i.e., the relation defined by Eq. (2) does not hold. Also, Eq. (2) neglects flux fringing and leakage. It is expected that flux fringing and leakage play a role in the flattening trend of the damping ratio when the current increases [20]. It is also noted that the damping ratio for current stepping up differs from that for current stepping down. This phenomenon is due to the hysteresis nature of ferromagnetic materials. The static hysteresis characteristic can be modeled by the classical Preisach model [21]. However, the investigation of this phenomenon was beyond the scope of the present study.

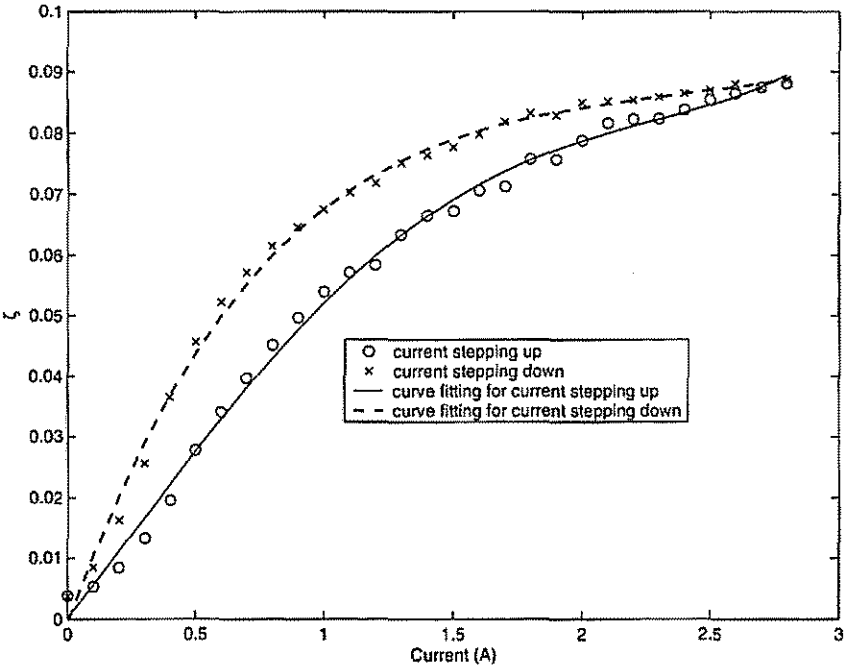

Figure 3. Relation between the damping ratio and the current of the coil.

The experiments were also conducted using three different system set-ups: case one $m = 0.0954$ kg, $f_n = 18.07$ Hz; case two $m = 0.15$ kg, $f_n = 15.03$ Hz; case three $m = 0.265$ kg, $f_n = 12.70$ Hz. All the tests were conducted with current stepping up. Tables 1 lists the results. The damping coefficients in Table 2 were computed by

$$c = 2m(2\pi f_n)\zeta \tag{4}$$

where ζ is given in Table 1. It is noted that for a given current, the damping coefficient c is not constant, but varies when the frequency of oscillation changes. This contradicts Eq. (3). In [17], a more elaborate model was used to describe the magnetic damping. The damping coefficient is found to be given by

$$c = \frac{l^2 B^2 R}{R^2 + \omega_n^2 L^2} \tag{5}$$

where l is the vertical height of the conductor immersed in the magnetic field, R is the resistance that eddy current encounters along the entire closed loop and L is the inductance of the loop. According to this relation, for a given magnetic field and conductor, the smaller the frequency of oscillation, the greater the damping coefficient. This agrees with the experimental results. The study reported in [17] also showed that electromagnetic damping tends to increase the effective restoring force such that an increase of electromagnetic damping results in an increase of the natural frequency. In the experiment, it was also observed that with an increase of the current, the natural frequency was increased slightly.

Table 1. Damping ratios for three testing cases.

Testing case	$I=0$ A	$I=.5$ A	$I=1.0$ A	$I=1.5$ A	$I=2.0$ A	$I=2.5$ A
one	4.303E-3	3.196E-2	6.156E-2	7.795E-2	8.980E-2	9.763E-2
two	3.820E-3	2.775E-2	5.407E-2	6.810E-2	7.880E-2	8.540E-2
three	3.373E-3	2.529E-2	4.677E-2	5.960E-2	6.835E-2	7.303E-2

Table 2. Damping coefficients (Ns/m) for three testing cases.

Testing case	$I=0$ A	$I=.5$ A	$I=1.0$ A	$I=1.5$ A	$I=2.0$ A	$I=2.5$ A
one	0.0932	0.6920	1.3328	1.6877	1.9441	2.1137
two	0.1087	0.7893	1.5380	1.9373	2.2416	2.4293
three	0.1427	1.0700	1.9791	2.5218	2.8919	3.0902

3. Comparison of two Different Damped DVAs

For the experimental system, the clamped-clamped beam plus the support of the absorber system is considered to be the primary system. An impact testing conducted on the primary system indicated that the first three natural frequencies are 15.1, 53.0, and 94.7 Hz. The inherent damping of the system is very low, about 0.3%. After the absorber system is attached to the primary system and the natural frequency of the absorber system is tuned to be 15.1 Hz, the first four natural frequencies of the entire system are 11.7, 19.1, 50.7, and 94.1 Hz. It is noted that the presence of modes higher than two in the responses is very weak and the system behaves strongly like a 2-DOF system. To simplify the analysis, the primary system is modeled as a lumped mass and stiffness system. The purpose of adding the DVA system is to suppress the beam vibration at the first natural frequency 15.1 Hz.

Figure 4 shows two damped DVA systems subjected to a harmonic force $F_0\sin(\omega t)$ where m and k denote the mass and stiffness of the primary system, respectively, m_a and k_a denote the mass and stiffness of the absorber system, respectively, and F_0 and ω are the force amplitude and exciting frequency, respectively. Figure 4(a) represents a common usage of a DVA while Fig. 4(b) represents the present system. In [14], the model shown in Fig. 4 (a) is referred to as groundhook tuned mass damper. In the study of active suspension systems, the damper connected as shown in Fig. 4(b) is called as skyhook damper [22]. To distinguish these two models, the models of Figs. 4(a) and 4(b) are referred to as groundhook DVA and skyhook DVA, respectively. However, it should be noted that the objective of using the damper for a vibration absorber is different from that of using a skyhook damper for active suspension systems. The dynamics of the groundhook DVA has been well known [1, 23]. As the skyhook DVA is not as common as the groundhook DVA, a natural question arises: how the performance of the skyhook DVA differs from that of the groundhook DVA? The following study serves two purposes: to understand the dynamics of the skyhook DVA and to compare the performance of the groundhook DVA with that of the skyhook DVA.

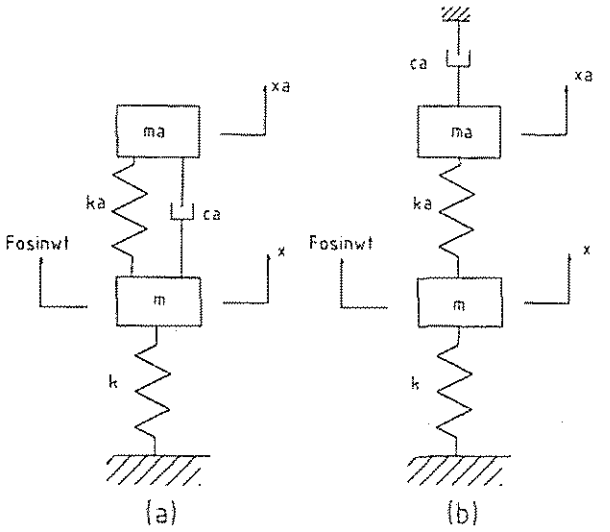

Figure 4. Schematics of the models: (a) groundhook DVA; (b) skyhook DVA.

The equation of motion for both the models is given as

$$\begin{bmatrix} m & 0 \\ 0 & m_a \end{bmatrix}\begin{bmatrix} \ddot{x} \\ \ddot{x}_a \end{bmatrix} + C\begin{bmatrix} \dot{x} \\ \dot{x}_a \end{bmatrix} + \begin{bmatrix} k+k_a & -k_a \\ -k_a & k_a \end{bmatrix}\begin{bmatrix} x \\ x_a \end{bmatrix} = \begin{bmatrix} F_0 \sin(\omega t) \\ 0 \end{bmatrix} \tag{6}$$

where the damping matrix C is of the form:

$$C = \begin{bmatrix} c_a & -c_a \\ -c_a & c_a \end{bmatrix} \text{ and } C = \begin{bmatrix} 0 & 0 \\ 0 & c_a \end{bmatrix} \tag{7}$$

for the groundhook DVA and the skyhook DVA, respectively. From a force viewpoint, the damping force of the groundhook DVA is proportional to the relative velocity between the absorber mass and primary mass and applied directly to both the masses while the damping force of the skyhook DVA is proportional to the absolute velocity of the absorber mass and applied directly to the absorber mass and the ground. Define the following symbols [24]

$$\omega_p = \sqrt{k/m},\ \omega_a = \sqrt{k_a/m_a},\ \beta = \omega_a/\omega_p,\ \mu = m_a/m,\ \zeta = c_a/(2m_a\omega_p),\ r = \omega/\omega_p$$

where ω_p is the natural frequency of the primary system without the absorber, ω_a is the natural frequency of the absorber system itself, μ is the mass ratio, ζ is the damping ratio, and r is the frequency ratio. The normalized amplitude of the steady-state response of the primary mass for the groundhook DVA is given as [24]

$$G = \left|\frac{Xk}{F_0}\right| = \sqrt{\frac{(2\zeta r)^2 + (\beta^2 - r^2)^2}{[1-(1+\mu)r^2]^2(2\zeta r)^2 + [(1-r^2)(\beta^2 - r^2) - \mu\beta^2 r^2]^2}}\ . \tag{8}$$

Following the same procedure given in [24], the normalized amplitude of the steady-state response of the primary mass for the skyhook DVA can be found to be

$$G=\left|\frac{Xk}{F_0}\right|=\sqrt{\frac{(2\zeta r)^2+(\beta^2-r^2)^2}{(1+\mu\beta^2-r^2)^2(2\zeta r)^2+[(1-r^2)(\beta^2-r^2)-\mu\beta^2 r^2]^2}}\,. \tag{9}$$

Using the following values: $m=1$ kg, $k=8900$ N/m, $m_a=0.15$ kg, the behaviors of the groundhook DVA and the skyhook DVA are compared both for the constant tuning and the optimum tuning. The constant tuning is defined as $\beta=1$ [1]. Figure 5 shows a comparison of the normalized amplitudes for the groundhook DVA and those for the skyhook DVA for three different damping ratios. It can be seen that both the models behave similarly: G reaches the minimum at $\beta=1$ and the larger the damping ratio, the smaller G at the resonances.

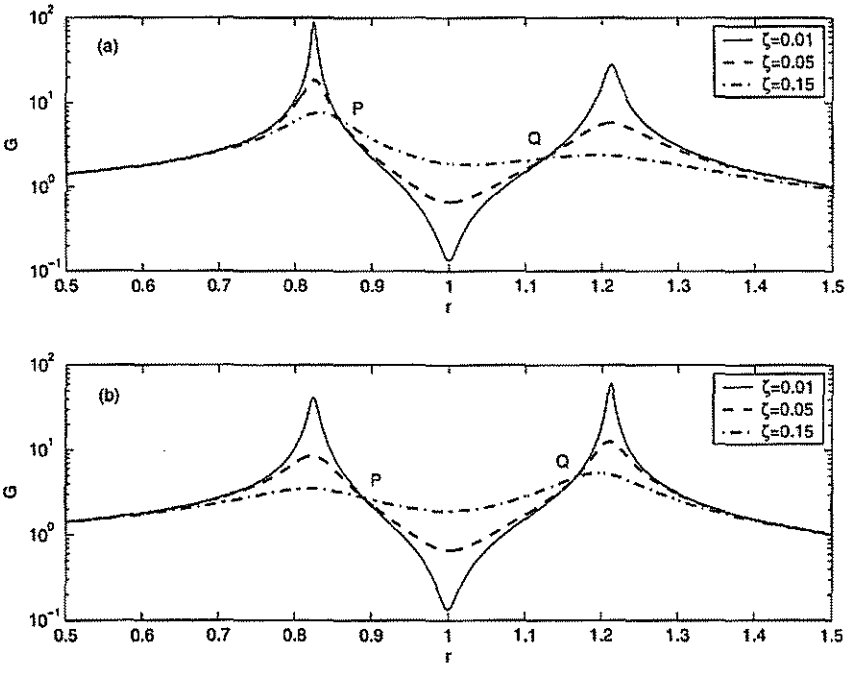

Figure 5. Normalized amplitudes: (a) the groundhook DVA; (b) the skyhook DVA.

A common feature of Fig. 5 is that there exist two fixed points P and Q through which each curve passes. This indicates that for given values of μ and β, there are two values of r which yield a value of G, independent of ζ. If r_1 denotes the frequency ratio corresponding point P and r_2 the frequency ratio corresponding to the point Q, the optimum tuning β^* is defined a value such that $G(r_1)=G(r_2)$. The optimum tuning conditions for the groundhook DVA are well known [23]. They are defined by the optimum tuning parameter

$$\beta^*=\frac{1}{1+\mu} \tag{10}$$

and the optimum damping ratio

$$\zeta_{opt} = \sqrt{\frac{3\mu}{8(1+\mu)^3}}. \tag{11}$$

The first two authors of this paper have derived the formulas to determine r_1, r_2, β^*, and ζ_{opt} for the skyhook DVA [25], which are given below. When the frequency ratios are determined by

$$r_{1,2} = \sqrt{\frac{1+(1+\mu)\beta^2 \mp \sqrt{1+2(\mu-1)\beta^2+(\mu^2+1)\beta^4}}{2}}, \tag{12}$$

the normalized amplitude for points P and Q is given as

$$G = \sqrt{\frac{1}{(1+\mu\beta^2-r^2)^2}}. \tag{13}$$

The optimum tuning condition is given as

$$\beta^* = \frac{1}{\sqrt{1-\mu}}. \tag{14}$$

The optimum damping ratio is given as

$$\zeta_{opt} = \frac{1}{2}\sqrt{\frac{3\mu}{(1-\mu)(2-\mu)}}. \tag{15}$$

Using the numerical values given above, it is found that $\beta^* = 0.8714$ for the groundhook DVA and $\beta^* = 1.083$ for the skyhook DVA. Figure 6 compares the normalized amplitudes vs. the frequency ratio when the absorber is tuned with β^*. It is noted that the minimum vibration occurs at β^*. Thus the absorber frequency should be chosen to be $\omega_a = \beta^* \omega_p$, i.e., anti-resonance frequency. Comparison of Figs. 5 and 6 shows a major difference between the constant tuning and the optimum tuning: with the optimum tuning, two peaks become almost equal in height. With the optimum tuning and the optimum damping ratio, the normalized amplitudes for both the models appear flat over a wide range. Such a feature allows a damped DVA to operate over a wide frequency range. However, this benefit is gained by scarifying the performance at the anti-resonance frequency. Figure 7 gives a comparison of the normalized amplitudes at the anti-resonance frequency. It is noted that for a given damping ratio, the damper in the skyhook DVA causes less increase in vibration. Figure 8 compares the maximum normalized amplitudes. The maximum normalized amplitude occurs at one of the resonance frequencies when the damping ratio is low or at the anti-resonance frequency when the damping is high. It is noted that when the damping is low, the groundhook DVA offers a slightly greater suppression of vibration than the skyhook DVA. However, when the damping is moderate or high, both the models perform similarly.

The above study has shown that the groundhook DVA and the skyhook DVA behave similarly. This fact indicates that although the developed tunable damper is used in a skyhook damper manner, the findings obtained from this study are still applicable if the same damper is used in a groundhook manner.

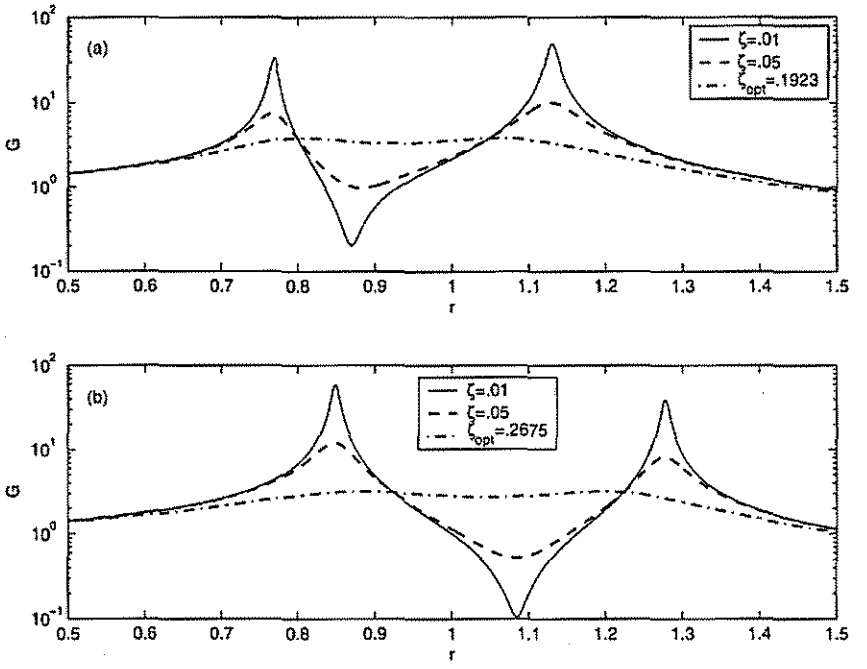

Figure 6. Normalized amplitudes for the optimum tuning with β^*: (a) the groundhook DVA; (b) the skyhook DVA.

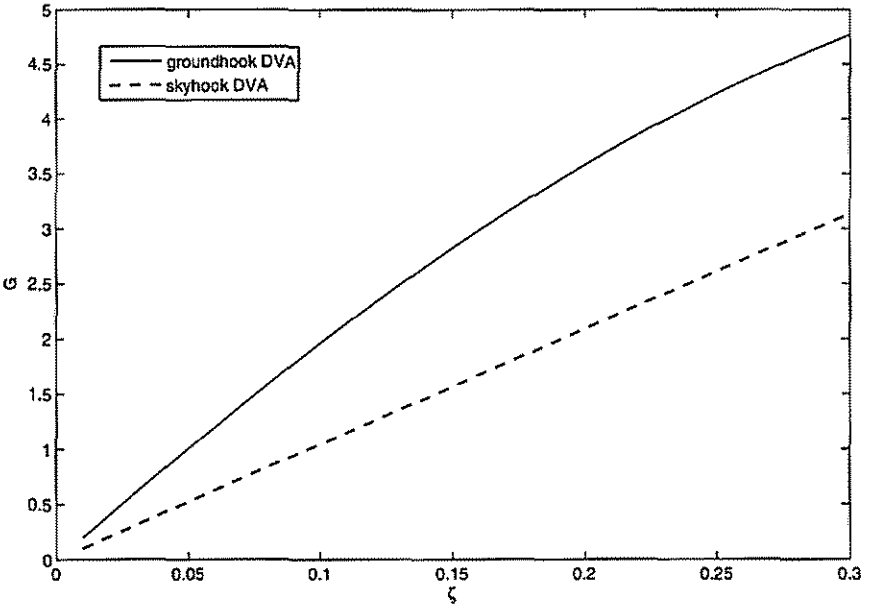

Figure 7. Normalized amplitudes at anti-resonance.

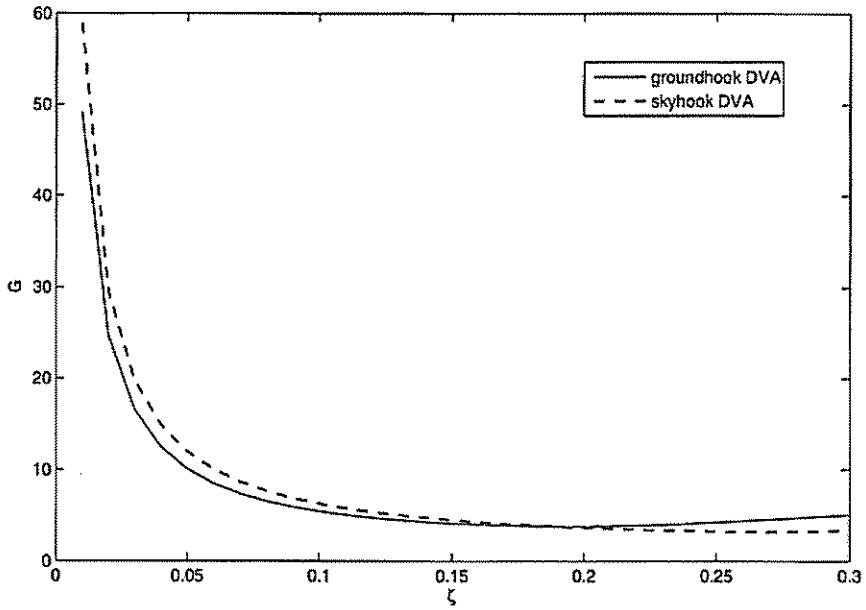

Figure 8. Maximum normalized amplitude.

4. CONTROL ALGORITHMS AND EXPERIMENT

The above study reveals that whether to use the damper depends on the location of the frequency ratio with respect to the fixed points P and Q (Fig. 5). The information about the fixed points consists of the corresponding exciting frequencies and the corresponding vibration magnitudes. Such information can be found analytically or experimentally beforehand. Hereafter, the frequencies corresponding to the points P and Q are referred to as crossing frequency and are denoted by f_P for point P and f_Q for point Q. If the crossing frequencies f_P and f_Q are known, a control algorithm based on the fast Fourier transform (FFT) can be used [19]. Assume that the natural frequencies of the entire system are f_{n1} and f_{n2} where $f_{n1} < f_{n2}$. A lower frequency bound f_1 is chosen to be a value much smaller than f_{n1} such that the damping has little effect on the magnitude of vibration. An upper frequency bound f_2 is chosen to be a value much greater than f_{n2} such that the damping has little effect on the magnitude of vibration. The FFT-based control algorithm contains the following steps:

1. Sample the response of the primary system over a specified time period with a sampling time Δt. The time period of each group of samples is chosen to be $T = N\Delta t$ where N is the number of samples.
2. Obtain the spectrum of the response by applying FFT to the sampled responses and find the frequency corresponding to the maximum magnitude of the spectrum. Let this frequency be the measured exciting frequency f.
3. If $f_1 < f < f_P + \Delta f$ or $f_Q - \Delta f < f < f_2$, turn on the damper power supply, otherwise turn off the damper power supply. Go to Step 1.

where Δf is the FFT spectrum resolution that is equal to $\Delta f = 1/T$. Considering that FFT may not be able to pinpoint a frequency, the region enclosed by f_P and f_Q is reduced by $2\Delta f$ such that the damper is turned off only when it is absolutely necessary.

A major shortcoming of the FFT-based algorithm is computational time. The data length should be long enough to have a sufficient frequency resolution. A longer data length means a slower reaction. For example, if $\Delta t = 0.001$ s and $N = 2048$ are used, $\Delta f = 0.4883$ Hz and $T = 2.048$ s. This study proposes a new control strategy which is based on the information about magnitudes of the steady-state response of the primary mass at the crossing frequencies. Magnitude of vibration is measured by a root mean squared (*rms*) value defined as

$$rms = \sqrt{\frac{\sum_{i=1}^{N} v_a^2(i)}{N}} \tag{16}$$

where $v_a(i)$ is the sampled acceleration signal and N is the number of samples of interest. Let rms_P denote the *rms* value of the response when the system is excited by f_P and rms_Q denote the *rms* value of the response when the system is excited by f_Q. The rms-based control algorithm contains the following steps:

1. Sample the response of the primary system over a specified time period.
2. Compute *rms* using the sampled data.
3. If $rms > rms_P$ or $rms > rms_Q$, turn on the damper power supply, otherwise turn off the damper power supply. Go to Step 1.

An experimental study was conducted to compare the performance of the two control algorithms. To this end, the absorber system was set up such that the absorber mass was $m_a = 0.15$ kg and the absorber frequency was tuned to be $f_a = 15.1$ Hz, i.e., the natural frequency of the primary system. The values of f_P, f_Q, rms_P, and rms_Q were found by the following way. With the damper current set to a constant value, the primary beam was excited at a frequency ω until the response became steady. Then the amplitude V_a of the steady-state acceleration signal was measured. The exciting frequency was increased by a step size of 0.2 Hz and the experiment was repeated. For each given damper current, the exciting frequencies were swept through 9.5 Hz to 20.5 Hz. The experiment was repeated for three different damper currents. The results are shown in Fig. 9. In Fig. 9(b), the amplitude V_d of the steady-state displacement signal was computed by $V_d = V_a/\omega^2$. From the figures, the crossing frequencies were found to be $f_P = 12.9$ Hz and $f_Q = 17.9$ Hz. The figures also reveal that the natural frequencies of the entire system were $f_{n1} = 11.7$ Hz and $f_{n2} = 19.1$ Hz. From the steady-state responses at the crossing frequencies, the *rms* values were found to be $rms_P = 0.021$ and $rms_Q = 0.039$.

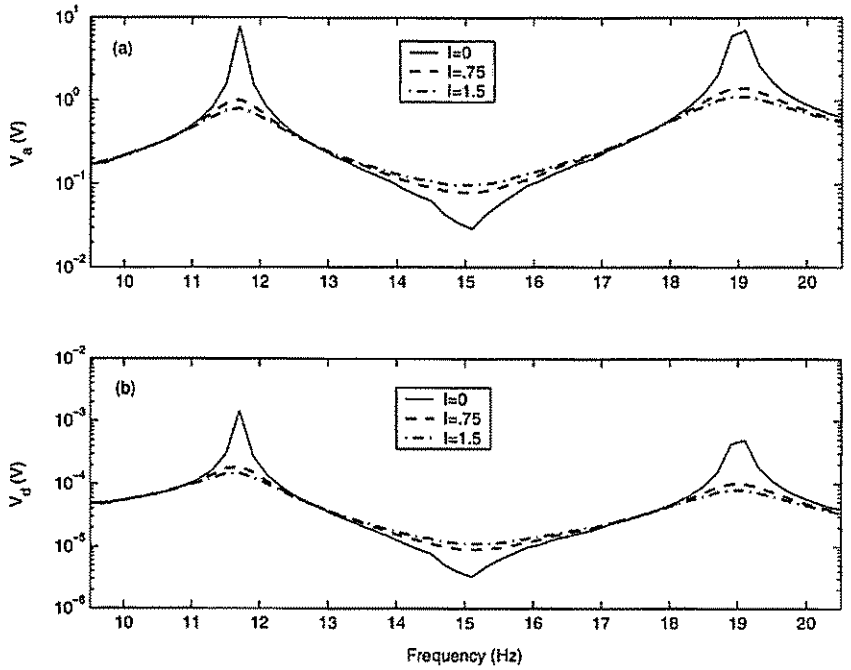

Figure 9. Amplitudes of the steady-state responses of the experimental system: (a) acceleration signal; (b) displacement signal.

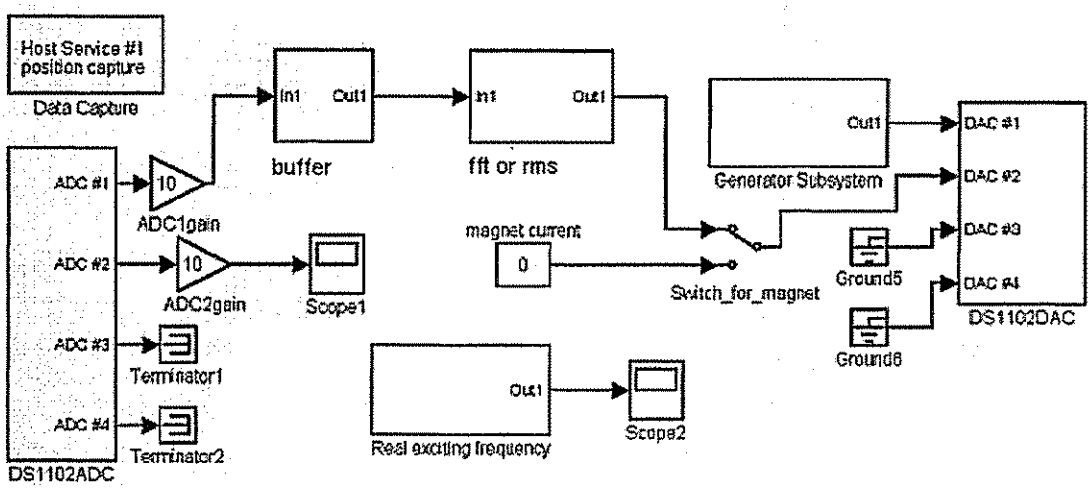

Figure 10. Simulink model for the on-line tuning test.

Figure 10 shows the Simulink model developed to test the tuning algorithms. Through the analog to digital channel ADC #1, the amplified accelerometer signals of the primary mass are sampled. An S function named "buffer" is used to collect the samples for a specified length such as $N = 2048$. For the FFT-based algorithm, this group of the data is transferred to an S function named "fft" where FFT is conducted and the peak frequency is found. Through the digital to analog channel DAC #2, the output of this S function is sent to the damper current control circuitry. For the 2nd algorithm, this group of the data is transferred to an S function named "rms" where the *rms* value of the sampled data is computed.

Through the digital to analog channel DAC #2, the output of this S function is sent to the damper current control circuitry. The exciting signal is generated by a sub-function block named "exciting signal" and output to the power amplifier through DAC #1. The acceleration signal of the absorber mass is sampled through ADC #2. This signal is used only for the purpose of reference.

Three testing scenarios were devised to test the control algorithms. The first scenario is a multi-step change in the exciting frequency. The exciting frequency was set to be 11.7 Hz or $f = f_{n1}$ for a period of 10 seconds. At $t = 10$ s, the exciting frequency was changed to be 15.1 Hz or $f = f_a$ for a period of 10 seconds. At $t = 20$ s, the exciting frequency was changed to be 19.1 Hz or $f = f_{n2}$ for another 10 seconds. This scenario was deliberately designed to set the system into resonance and anti-resonance during the different periods. Figure 11(a) shows the response of the primary beam when the damper control was not activated and Fig. 11(b) shows the variation of the exciting frequency. It can be seen that the response was increasing during the periods of the first 10 seconds and the last 10 seconds as the system was at resonance. During the period of $10 < t < 20$ s, the response was decreasing because the exciting frequency was equal to the absorber frequency, i.e., anti-resonance frequency. Figure 12 shows the results when the damper was controlled using the FFT-based method. The data length was chosen to be $N = 2048$ and $f_1 = 10$ Hz and $f_2 = 21$ Hz were used. Figure 12(b) indicates that it took 2.048 second to find the measured exciting frequency and at $t = 2.048$ s, the damper was turned on. As shown in Fig. 12(a), after the damper was turned on, the response was quickly suppressed. When the exciting frequency was switched to be the anti-resonance frequency, the response was further reduced. However, as indicated in the figure, the response did not reach the minimum level until the measured exciting frequency was found to be within the crossing frequencies and the damper was turned off. At $t = 20$ s when the exciting frequency was switched to be the second natural frequency, the response started to increase as the damper was off. After the damper was turned on again based on the new measured exciting frequency, the response was suppressed to the minimum level. Figure 13 shows the results when the second algorithm was used. The number of the data used to compute the *rms* value was $N = 512$. Because a shorter data length was used, the control system reacted quickly and the damper was promptly turned on/off as needed.

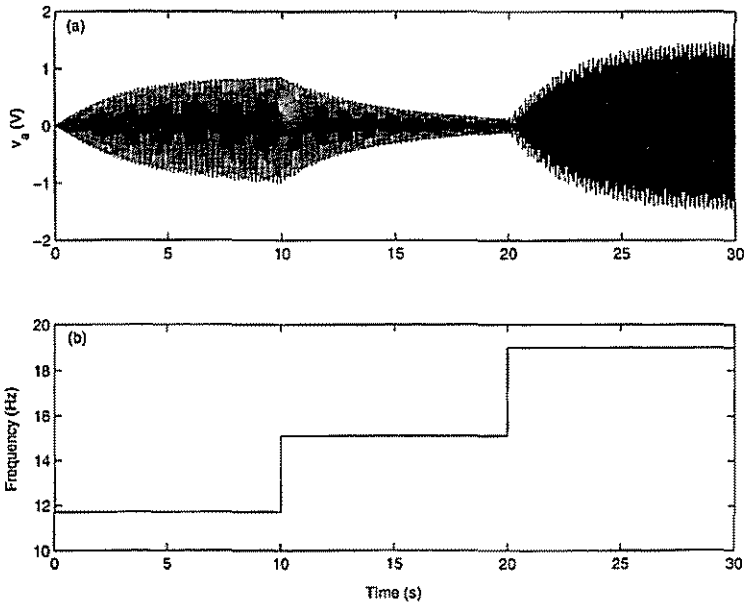

Figure 11. Testing scenario one: (a) response of the primary beam without damper control; (b) the exciting frequency.

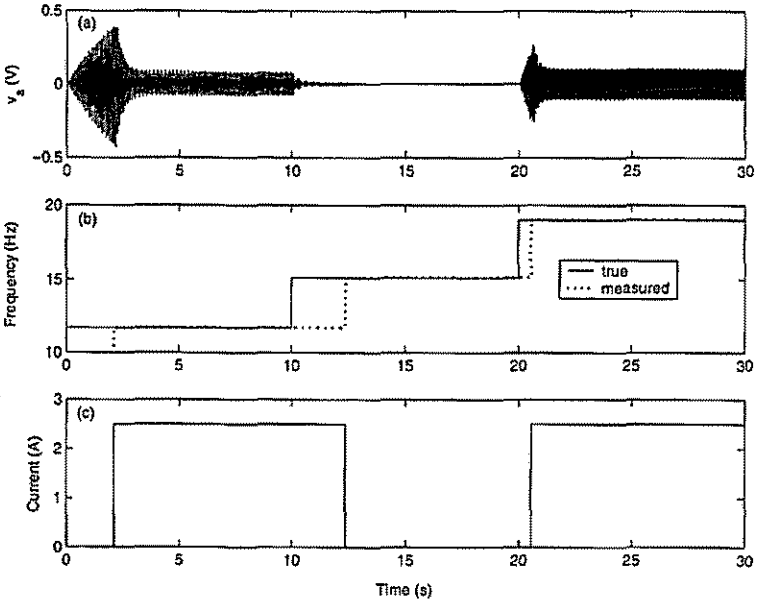

Figure 12. Results of the testing scenario one using the FFT-based algorithm: (a) response; (b) the true and measured exciting frequencies; (c) the damper current.

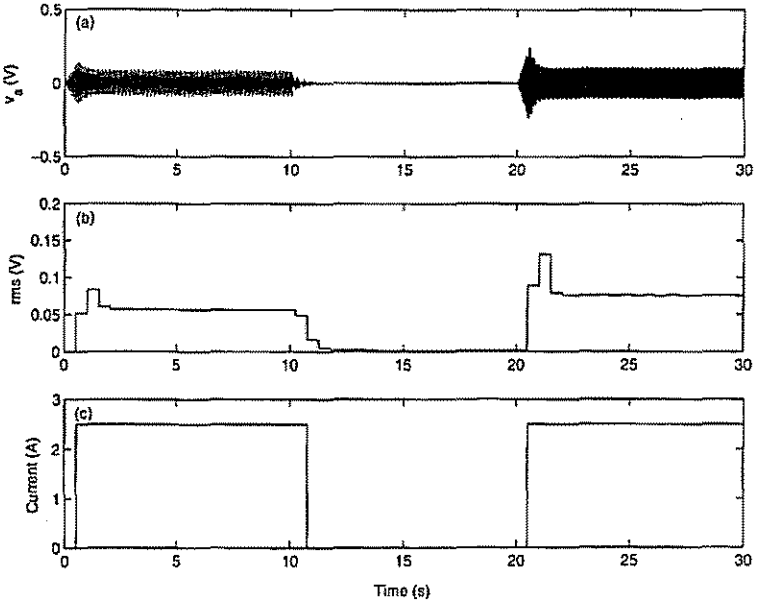

Figure 13. Results of the testing scenario one using the rms-based algorithm: (a) response; (b) the *rms* value of the response; (c) the damper current.

The second testing scenario was a linear change in the exciting frequency. For the period of $0 \le t < 10$ s, the exciting frequency was 10 Hz. During the period of $10 \le t \le 30$ s, the exciting frequency was linearly increased from 10 Hz to 15.1 Hz. Figure 14(a) shows the response without control of the damper while Fig. 14(b) shows the variation of the exciting frequency. It can be seen that when $t < 10$ s,

the response was small since the exciting frequency was away from the natural frequencies. However, it is noted that the transient present in the response sustained for a long duration as the damping was lower. When the exciting frequency was linearly increased, the response went through an interesting varying pattern and eventually reached the minimum level after the exciting frequency was equal to the anti-resonance frequency and the transient response died out. Figure 15 shows the results when the damper was controlled using the FFT-based algorithm. At $t = 2.048$ s, the damper was turned on and the transient response was quickly suppressed. It should be noted that when the exciting frequency was varying linearly, the peak frequency of the FFT spectrum did not correspond to the true exciting frequency. Figure 16 shows the results using the rms-based algorithm. Comparison of Figs. 15(c) and 16(c) reveals a major difference between the two methods. With the FFT-based control algorithm, the damper was turned on for a period longer than needed.

The third testing scenario consisted of the first step change in scenario one and an impact disturbance applied at about $t = 20$ s. Figure 17 shows the results when the damper was controlled using the FFT-based algorithm. As an impact caused the transient response, the peak frequency of the FFT spectrum corresponded to the second natural frequency and the damper was turned on until the exciting frequency became dominant again. Figure 18 shows the results using the rms-based algorithm. Once again, it can be seen that the rms-based algorithm resulted in a quicker reaction and a shorter damper activation.

Up to this point, control of the damper has been an on/off action. With the rms-based algorithm, a proportional control was tested. The damper current was computed by

$$I = \begin{cases} 0 & \text{if } rms \le 0.021 \\ g\dfrac{rms - 0.021}{0.021} & \text{if } 0.021 < rms < 0.021(2.5/g + 1) \\ 2.5 & \text{if } 0.021(2.5/g + 1) \le rms \end{cases} \tag{17}$$

where g is the control gain. Note that in the above equation, $rms_p = 0.021$ is used as the threshold value for the rms value and $I = 2.5$ A is used as the maximum current. Figure 19 shows the results for the testing scenario one when three different gains were used. When the gain g exceeded 1.899, the control action became on/off and vibration suppression was the fastest. With a smaller gain, the damper was partially turned on and vibration suppression was relatively slower.

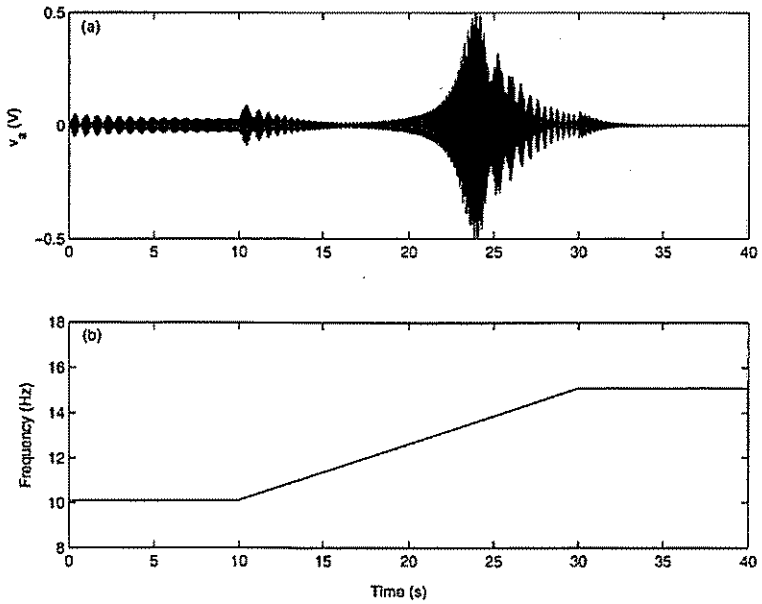

Figure 14. Testing scenario two: (a) response of the primary beam without control of the damper; (b) the exciting frequency.

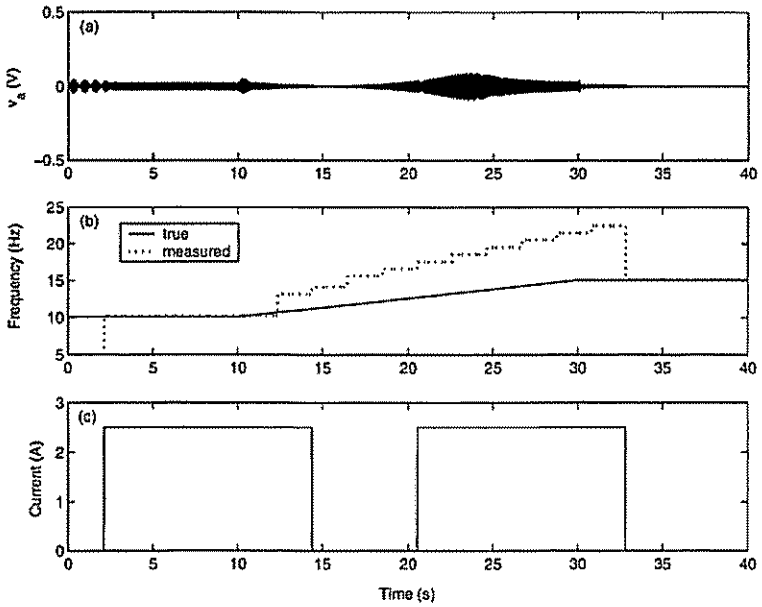

Figure 15. Results of the testing scenario two using the FFT-based algorithm: (a) response; (b) the true and measured exciting frequencies; (c) the damper current.

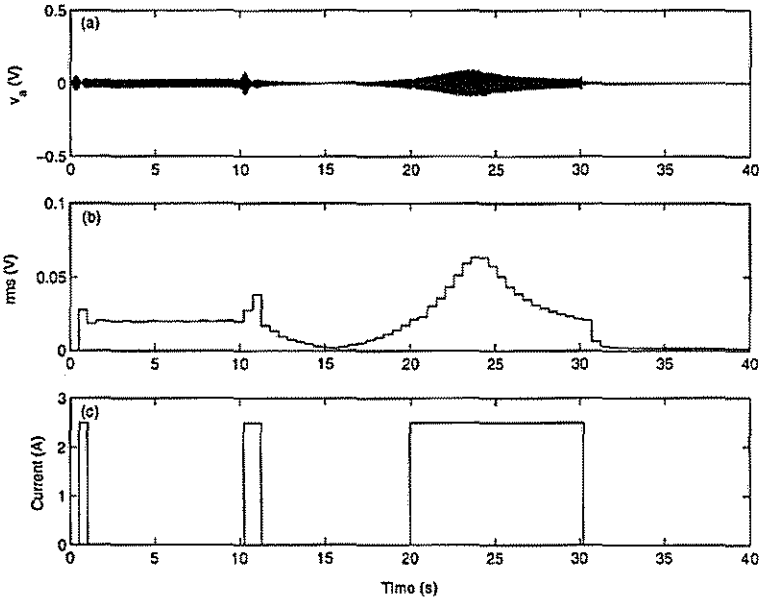

Figure 16. Results of the testing scenario two using the rms-based algorithm: (a) response; (b) the *rms* value of the response; (c) the damper current.

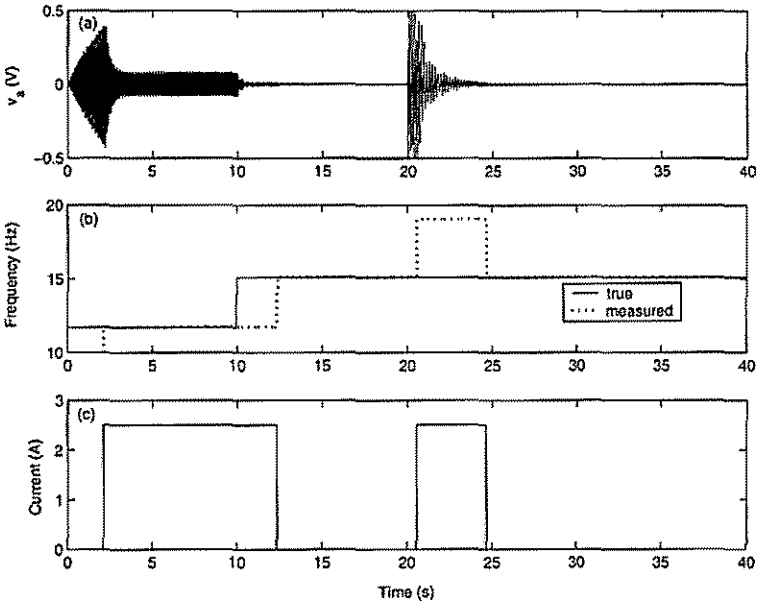

Figure 17. Results of the testing scenario three using the FFT-based algorithm: (a) response; (b) the true and measured exciting frequencies; (c) the damper current.

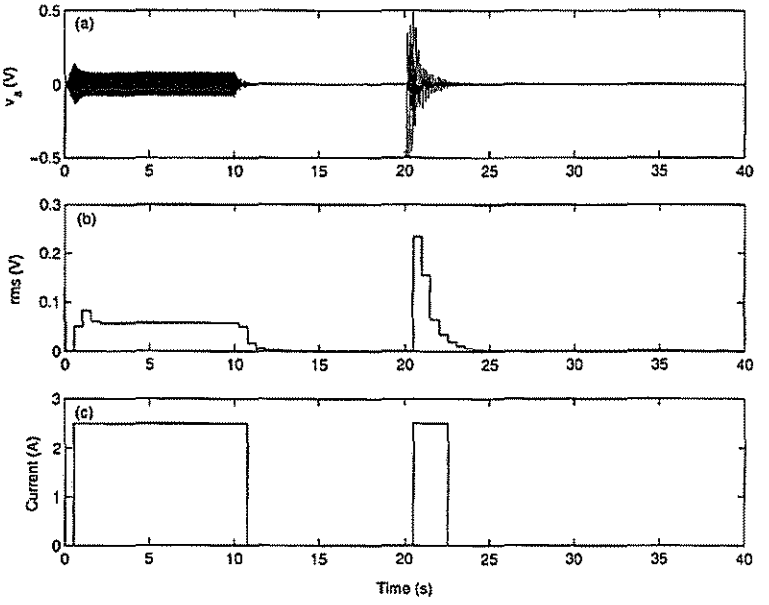

Figure 18. Results of the testing scenario three using the rms-based algorithm: (a) response; (b) the *rms* value of the response; (c) the damper current.

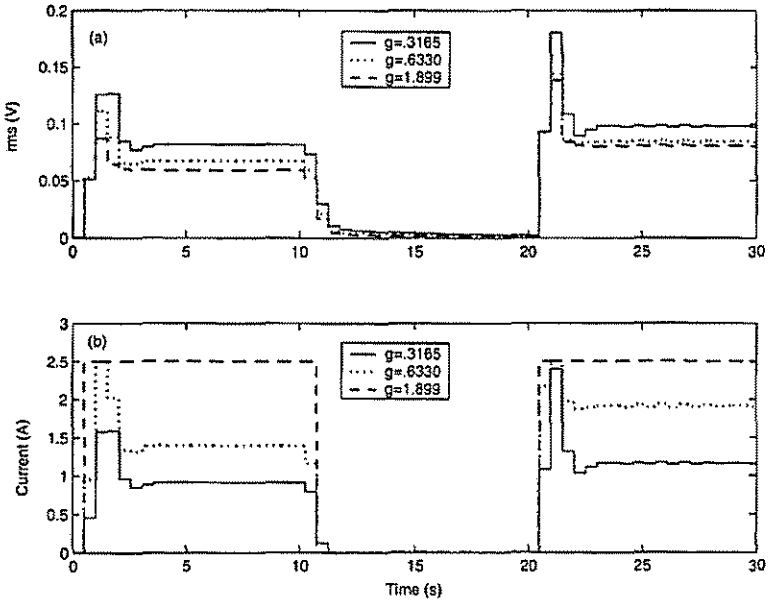

Figure 19. Testing results for scenario one using the rms-based algorithm with a proportional control: (a) the *rms* values of the responses; (b) the damper currents.

5. Conclusion

An electromagnetic damper has been developed. Based on the eddy-current phenomenon, the electromagnetic damper can change its damping value by varying the current to the electromagnet. Using the developed damper, a tunable damped dynamic vibration absorber has been constructed. The tunable dynamic vibration absorber can be used to suppress vibration of a structure subjected to a harmonic excitation with a variable frequency. The damper is used to form a skyhook DVA. The performance of

the skyhook DVA has been compared with that of the groundhook DVA. The study has indicated that for both the constant tuning and the optimum tuning, the groundhook DVA and skyhook DVA perform similarly. This conclusion is of significance as the skyhook DVA offers an alternative way to apply the damper or test the damper. Auto-tuning of the damper to cope with a variable exciting frequency has been studied. A previously developed FFT-based tuning algorithm has been introduced. A new rms-based tuning algorithm has been proposed. Three testing scenarios have been used to test the effectiveness of the two tuning algorithms. The experimental results have shown that the developed damper is able to achieve the desired goal: applying the maximum damping if the system is excited at about the natural frequencies and maintaining a passive vibration absorber if the system is excited at about the anti-resonance frequency. With the developed vibration absorber, vibration suppression can be accomplished in a fast, no mechanical contact, and no moving-part manner. The study has shown that the rms-based tuning algorithm performs better than the FFT-based tuning algorithm in terms of reaction time and simplicity of implementation. It should be noted that another advantage of the developed tunable damped vibration absorber is its stability because the actuation of the damper only dissipates vibration energy, i.e., the entire system will not become unstable due to the activation of the damper.

6. ACKNOWLEDGEMENT

The authors wish to acknowledge the support of the National Science and Engineering Research Council of Canada under the grant No. OGP-0184068.

REFERENCES

[1] Den Hartog JP, *Mechanical Vibrations*. New York: Dover Publications, Inc., 1985.

[2] Franchek MA, Ryan MW, Bernhard RJ, Adaptive passive vibration control, *Journal of Sound and Vibration* 1995; 189(5):565-585.

[3] Nagaya K, Kurusu A, Ikai S, Shitani Y, Vibration control of a structure by using a tunable absorber and an optimal vibration absorber under auto-tuning control, *Journal of Sound and Vibration* 1999, 228(4):773-792.

[4] Varadarajan N., Nagarajaiah S, Response control of building with variable stiffness tuned mass damper using empirical mode decomposition and Hilbert transform algorithm, *Proceedings of 16th ASCE Engineering Mechanics Conference*, Seattle; 2003.

[5] Liao L, Study of two different tunable vibration absorbers: variable stiffness absorber and variable damping absorber. *MS thesis*, Lakehead University, Thunder Bay, 2004.

[6] Olgac N., Hilm-Hansen BT, A novel active vibration absorption technique: delayed resonator. *Journal of Sound and Vibration* 1994; 176(1):93-104.

[7] Kidner M, Brenan MJ, Improving the performance of a vibration neutraliser by actively removing damping. *Journal of Sound and Vibration* 1999; 221(4):587-606.

[8] Patten WN, Sack RL, He Q, Controlled semiactive hydralic vibration absorber for bridges. *Journal of Structural Engineering* 1996; 122(2):187-192.

[9] Symans MD, Constantinou MC, Seismic testing of a building structure with a semi-active fluid damper control system. *Earthquake Engineering and Structural Dynamics* 1997; 26(7):759-777.

[10] Kannan S, Uras HM, Aktan HM, Active control of building seismic response by energy dissipation, *Earthquake Engineering and Structural Dynamics* 1995; 24(5):747-759.

[11] Ketema Y, A viscoelastic dynamic vibration absorber with adaptable suppression band: a feasibility study. *Journal of Sound and Vibration* 1998; 216(1):133-145.

[12] Symans MD, Constantinou M, Semi-active control systems for seismic protection of structures: a state-of-art review. *Engineering Structures* 1999; 21(6):469-487.

[13] Stanway R, Sporston JL, El-Wahed AK, Applications of electrorheological fuilds in vibration control: a survey. *Smart Materials and Structures* 1996; 5(4):464-482.

[14] Setareh M, Floor vibration control using semi-active tuned mass dampers. *Canadian Journal of Civil Engineering* 2002; 29:76-84.
[15] Yamshita S, Seto K, Vibration and noise control using dual dynamic absorbers with magnetic damping. *Proceedings of the third International Isem Symposium on the Application of Electromagnetic Forces*, Sendai, 1992.
[16] Kienholz D, Pendleton S, Demonstration of solar array vibration suppression, *SPIE* 1994; 2193:59-72.
[17] McCarthy L, On the electromagnetically damped mechanical harmonic oscillator. *American Journal of Physics* 1996; 64:885-891.
[18] Graves KE, Toncich D, Ioveniti PG, Theoretical comparison of motional and transormer emf device damping efficiency. *Journal of Sound and Vibration* 2000, 233(3):441-453.
[19] Liao L, Liu K, Control of Structural Vibration Using a Variable Damping Vibration Absorber. *Proceedings of the CSME 2004 Forum*, London, Canada, 2004.
[20] Sarma M. S., Electric Machines: Steady-state Theory and Dynamic Performance, West Publishing Company, St. Paul, 1994.
[21] Mayergoyz, I. D., *Mathematical Models of Hysteresis*, Springer: New York, 1991.
[22] Karnopp D, Crosby MJ, Harwood RA, Vibration control using semiactive force generators. *Transactions of ASME, Journal of Engineering for Industry* 1974; 96:619-626.
[23] Brock JE, A note on the damped vibration absorber. *Transactions of ASME, Journal of Applied Mechanics* 1946; 68:284.
[24] Inman DJ, *Engineering Vibration*. 2nd Edition, New Jersey: Prentice-Hall, 2001.
[25] Liu, K., Liu, J., The damped vibration absorbers: revisited and new result, *Journal of Sound and Vibration* 2005, 284:1181-1189.